JOURNAL OF THEORETICAL
AND APPLIED MECHANICS
63, 3, pp. 679–690, Warsaw 2025
https://doi.org/10.15632/jtam-pl/205304

IMPROVED HYPERELASTIC MATERIAL CHARACTERIZATION USING MEASUREMENT DATA PRE-PROCESSING

Zoltan KOVACS[1], Andras ANINGER[1*], Szabolcs BEREZVAI[2]

[1] *eCon Engineering Ltd, Budapest, Hungary*
[2] *Department of Applied Mechanics, Faculty of Mechanical Engineering, Budapest University of Technology and Economics, Budapest, Hungary*
*corresponding author, *andras.aninger@econengineering.com*

Mechanical characterization of elastomers is a long-studied but still challenging area. Finite element solvers offer a great variety of hyperelastic models; however, no straightforward selection process is provided. This paper presents a methodology for high-fidelity hyperelastic parameter fitting tailored for elastomers. One of its main components is a pre-processing module, which helps select the most suitable model based on all information extractable from the measured stress-strain curves. In this contribution, the concept of the pre-processing module is presented, while its efficiency is demonstrated through benchmark fitting processes using the Treloar dataset and an experimental dataset of an nitril butadiene rubber (NBR) specimen.

Keywords: hyperelasticity; elastomers; parameter-optimization.

1. Introduction

The mechanical characterization of elastomers and rubber-like materials is a long-researched but still challenging area in the field of solid mechanics. These materials exhibit large strains and displacements during loading, while the stress-strain curve can be highly nonlinear (Bergström, 2015; Treloar, 2005). For the constitutive modelling of the elastic behavior of elastomers, the so-called hyperelastic constitutive models can be adopted. This modelling approach is a phenomenological approach, where a suitable strain energy function is to be fitted simultaneously to the experimental data from various load cases (Holzapfel, 2010; Doghri, 2000).

The history of hyperelastic constitutive models is strongly connected to rubbers since the first hyperelastic strain energy functions were formulated by Mooney (1940) and Rivlin and Saunders (1951) to describe the behaviour of filled rubbers as the generalization of the Hooke's law for finite strains. Since then, a great variety of hyperelastic potentials were developed. Some rely on only mathematical considerations (e.g., the polynomial model family), while others are based on the micromechanical or microstructural description of the strongly crosslinked elastomers. Recently, He *et al.* (2022) summarized a total number of 85 formulations of hyperelastic strain energy potential both for incompressible (pure deviatoric) and for volumetric compression cases. Furthermore, concerning the fitting of the parameters of these models, the generalized Mooney space (GMS) approach for some specific hyperelastic potentials was recently proposed which

Ministry of Science and Higher Education
Republic of Poland

The publication has been funded by the Polish Ministry of Science and Higher Education under the Excellent Science II programme "Support for scientific conferences".
The content of this article was presented during the 40th Danubia-Adria Symposium on Advances in Experimental Mechanics, Gdańsk, Poland, September 24–27, 2024.

transforms the material testing curve into a polynomial space, where the fit can be performed more efficiently (Anssari-Benam *et al.*, 2022).

In the commercial finite element solvers (Ansys, Abaqus, Ls-Dyna), a great variety of hyperelastic models are available. However, no straightforward selection process is provided for the users. Since hyperelastic modelling and parameter fitting is a complex task, dedicated software solutions (e.g., MCalibration (Bergström, 2015), Hyperfit) are available as well to fit a suitably chosen hyperelastic strain energy potential to the material testing data. However, none of these dedicated software applications provides the user with constitutive model decision support, which is an essential decision in the material modeling process to be made prior to the fitting. In addition, industrial practice shows that the available measurement data are often incomplete and contradictory, and the average user does not have the expertise to confidently filter the data containing information about the complex material behaviour.

The research project "2020-1.1.2-PIACI-KFI-2021-00314" aims to develop a high-fidelity material parameter fitting methodology tailored for rubber-like material characterized by hyperelastic constitutive models. One of the main components of the fitting procedure is an automatic pre-processing module, which helps users select the most suitable material model using all information extractable from the measured stress-strain curves for different load cases and further available mechanical test data using techniques based on the theory of hyperelasticity.

In this paper, the concept of the pre-processing module is presented. Section 2 summarizes the theoretical background of hyperelasticity and the investigated hyperelastic models. Section 3 presents the concept of the pre-processing module and the applied methods. Section 4 is dedicated to the case studies, including 1) the classical Treloar dataset and 2) a self-made dataset for NBRs, including uniaxial tension and compression, planar tension and simple shear tests. Finally, the main findings of the case studies are presented in Section 5.

2. Theoretical background

The theory of hyperelasticity is based on the finite strain material formulation of kinematics, where a polyconvex scalar function $W(\mathbf{F})$ can be introduced expressing the stored strain energy per unit reference volume as the function of deformation gradient $\mathbf{F}$ or the right Cauchy–Green deformation tensor $\mathbf{C}$, namely $W(\mathbf{C})$. From this, the first Piola–Kirchhoff stress tensor ($\mathbf{P}$) can be directly derived from the strain energy function using

$$\mathbf{P} = \frac{\partial W(\mathbf{F})}{\partial \mathbf{F}}, \qquad \text{or} \qquad \mathbf{P} = 2\mathbf{F}\frac{\partial W(\mathbf{C})}{\partial \mathbf{C}}. \tag{2.1}$$

2.1. Isotropic hyperelastic models

In the case of isotropic material, the strain energy function can be expressed by either the function of the principal invariants of $\mathbf{C}$ (I_1, I_2, and I_3) or the principal stretches (λ_1, λ_2, and λ_3), namely $W(I_1, I_2, I_3)$ or $W(\lambda_1, \lambda_2, \lambda_3)$ (Holzapfel, 2010). The scalar invariants of $\mathbf{C}$ are defined as

$$I_1 = \mathrm{tr}(\mathbf{C}), \qquad I_2 = \frac{1}{2}\left(I_1^2 - \mathrm{tr}(\mathbf{C}^2)\right), \qquad I_3 = \det \mathbf{C} = J^2, \tag{2.2}$$

which can also be expressed using the principal stretches (λ_1, λ_2, and λ_3) as

$$I_1 = \lambda_1^2 + \lambda_2^2 + \lambda_3^2, \qquad I_2 = (\lambda_1\lambda_2)^2 + (\lambda_1\lambda_3)^2 + (\lambda_2\lambda_3)^2, \qquad I_3 = (\lambda_1\lambda_2\lambda_3)^2. \tag{2.3}$$

In this case, the Cauchy (σ_k) and the first Piola–Kirchhoff (P_k) principal stresses can also be expressed in a compact form as

$$\sigma_k = \frac{\lambda_k}{J}\frac{\partial W}{\partial \lambda_k}, \qquad P_k = \frac{\partial W}{\partial \lambda_k}, \qquad k = 1, 2, 3. \tag{2.4}$$

2.2. Incompressible hyperelastic model

Elastomers are commonly modeled as incompressible materials because their bulk modulus is extremely high, while the volumetric deformation is negligible. Assuming a perfectly incompressible material, where the volume is constant during loading, for the entire deformation

$$\det \mathbf{F} = J \equiv 1 \qquad \text{and} \qquad I_3 \equiv 1 \tag{2.5}$$

holds. Consequently, the strain energy potential simplifies to $W(I_1, I_2, I_3) = W(I_1, I_2)$. In this case, the stress tensor can be derived using the deviatoric and volumetric split as

$$\boldsymbol{\sigma} = \mathbf{s} + \mathbf{p}, \tag{2.6}$$

where $\mathbf{s} = \mathrm{dev}\boldsymbol{\sigma}$ is the deviatoric part and $\mathbf{p} = p\mathbf{I}$ is the volumetric stress term. In this case, the deviatoric stress can be derived from the $W(I_1, I_2)$ strain energy functions using the derivations in Eq. (2.4), while the unknown pressure p should be expressed from the boundary conditions (e.g., stress-free transverse stresses). Therefore, the principal stresses for the incompressible case simplify to

$$\sigma_k = \lambda_k \frac{\partial W}{\partial \lambda_k} + p, \qquad P_k = \frac{\partial W}{\partial \lambda_k} + \frac{p}{\lambda_k}, \qquad k = 1, 2, 3. \tag{2.7}$$

2.3. Strain energy functions

In the literature, a great variety of incompressible hyperelastic potentials are available (He *et al.*, 2022). However, in commercial finite element solvers, the number of models is limited. Some models are defined only using the first invariant I_1, and the strain energy potential can be expressed as $W(I_1)$. These models are the Neo–Hookean (NH) (Mooney, 1940), the Yeoh (Y) (Yeoh, 1990), the Arruda–Boyce (AB) (Arruda & Boyce, 1993), and the Gent models (G) (Gent, 1996; Gent & Thomas, 1958). The corresponding strain energy functions are defined as

$$W^{\mathrm{NH}} = C_{10}\left(I_1 - 3\right), \tag{2.8}$$

$$W^{\mathrm{Y}} = C_{10}\left(I_1 - 3\right) + C_{20}\left(I_1 - 3\right)^2 + C_{30}\left(I_1 - 3\right)^3, \tag{2.9}$$

$$W^{\mathrm{AB}} = \mu\left[\frac{I_1 - 3}{2} + \frac{I_1^2 - 9}{20\lambda_m^2} + \frac{11\left(I_1^3 - 27\right)}{1050\lambda_m^4} + \frac{19\left(I_1^4 - 81\right)}{7000\lambda_m^6} + \frac{519\left(I_1^5 - 243\right)}{673750\lambda_m^8}\right], \tag{2.10}$$

$$W^{\mathrm{G}} = C_0 \ln\left(1 - \frac{I_1 - 3}{I_m - 3}\right), \tag{2.11}$$

Some other models are also dependent on the second invariant I_2. Therefore, the hyperelastic potential in this form can be expressed as $W(I_1, I_2)$. These models are the Mooney–Rivlin (MR) (Rivlin & Saunders, 1951), the polynomial (P), and the Ogden (O) (Ogden, 1972):

$$W^{\mathrm{MR}} = C_{10}\left(I_1 - 3\right) + C_{01}\left(I_2 - 3\right), \tag{2.12}$$

$$W^{\mathrm{P}} = \sum_{i+j=1}^{N} C_{ij}\left(I_1 - 3\right)^i \left(I_2 - 3\right)^j, \tag{2.13}$$

$$W^{\mathrm{O}} = \sum_{i=1}^{N} \frac{2\mu_i}{\alpha_i^2}\left(\lambda_1^{\alpha_i} + \lambda_2^{\alpha_i} + \lambda_2^{\alpha_i} - 3\right). \tag{2.14}$$

It should be noted that some models are based on pure mathematical considerations (e.g., polynomial, Ogden, Yeoh), while others rely on statistical or micromechanical models (e.g., Gent,

Arruda–Boyce). On the other hand, these models are not independent since by selecting the material constants properly, the models reduce to each other. The hyperelastic models and their relations are summarized in Fig. 1.

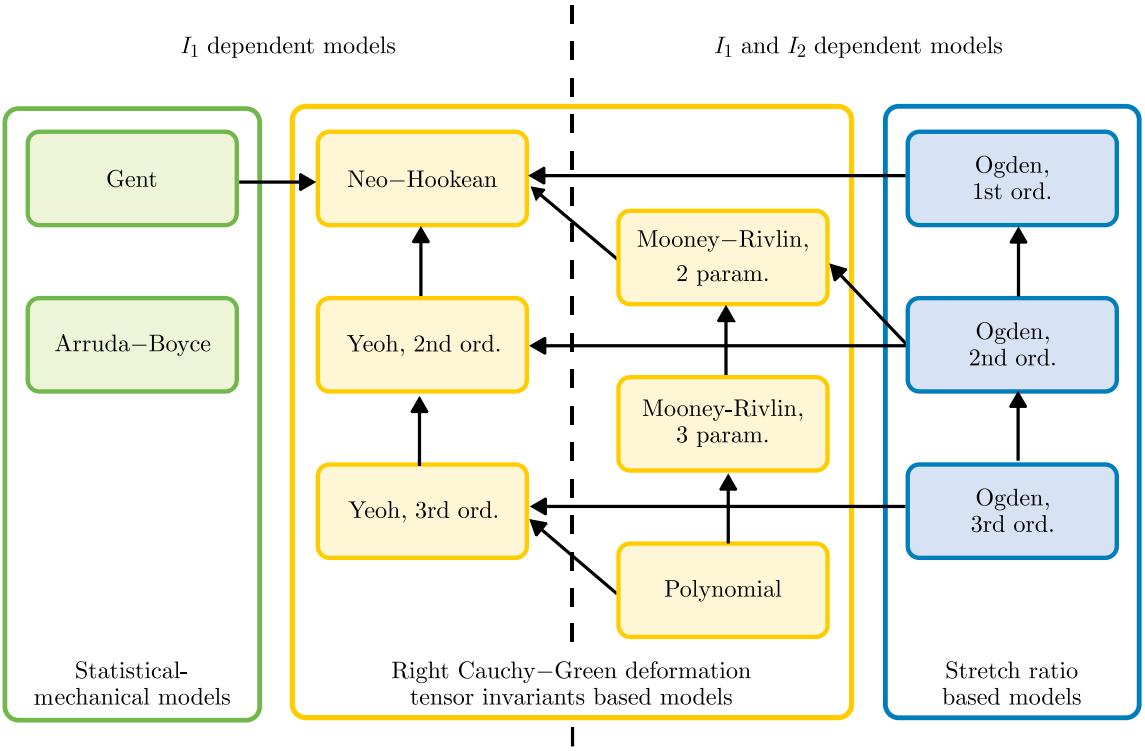

Fig. 1. Summary of the hyperelastic models available in the commercial finite element solvers.

2.4. Load cases

The hyperelastic potentials contain many material parameters that need to be fitted based on experimental data. For incompressible materials, four different load cases are distinguished: uniaxial (UA), biaxial (BA), planar (PL) and simple shear (SS). For these loading cases, the deformation gradient tensor $\mathbf{F}$, the volume ratio J and the first Piola–Kirchhoff stress tensor $\mathbf{P}$ or the Cauchy stress tensor $\boldsymbol{\sigma}$ can be obtained as:

– uniaxial tension/compression (UN):

$$\mathbf{F}^{\mathrm{UN}} = \begin{bmatrix} \lambda & 0 & 0 \\ 0 & \lambda_T & 0 \\ 0 & 0 & \lambda_T \end{bmatrix}, \qquad J^{\mathrm{UN}} = \lambda\lambda_T^2, \qquad \mathbf{P}^{\mathrm{UN}} = \begin{bmatrix} P & 0 & 0 \\ 0 & 0 & 0 \\ 0 & 0 & 0 \end{bmatrix}, \tag{2.15}$$

– biaxial tension/compression (BA):

$$\mathbf{F}^{\mathrm{BA}} = \begin{bmatrix} \lambda & 0 & 0 \\ 0 & \lambda & 0 \\ 0 & 0 & \lambda_T \end{bmatrix}, \qquad J^{\mathrm{BA}} = \lambda^2\lambda_T, \qquad \mathbf{P}^{\mathrm{BA}} = \begin{bmatrix} P & 0 & 0 \\ 0 & P & 0 \\ 0 & 0 & 0 \end{bmatrix}, \tag{2.16}$$

– planar tension/compression (PL):

$$\mathbf{F}^{\mathrm{PL}} = \begin{bmatrix} \lambda & 0 & 0 \\ 0 & 1 & 0 \\ 0 & 0 & \lambda_T \end{bmatrix}, \qquad J^{\mathrm{PL}} = \lambda\lambda_T, \qquad \mathbf{P}^{\mathrm{PL}} = \begin{bmatrix} P_1 & 0 & 0 \\ 0 & P_2 & 0 \\ 0 & 0 & 0 \end{bmatrix}, \tag{2.17}$$

– simple shear (SS):

$$\mathbf{F}^{\mathrm{SS}} = \begin{bmatrix} 1 & \gamma & 0 \\ 0 & 1 & 0 \\ 0 & 0 & 1 \end{bmatrix}, \qquad J^{\mathrm{SS}} = 1, \qquad \boldsymbol{\sigma}^{\mathrm{SS}} = \begin{bmatrix} \sigma_{11} & \sigma_{12} & 0 \\ \sigma_{12} & \sigma_{22} & 0 \\ 0 & 0 & 0 \end{bmatrix}. \tag{2.18}$$

3. Concept of data pre-processing

For modelling rubber-like elastomers, a large number of material models and parameter fitting procedures are available in the literature. However, all these methods assume that the user has a precise knowledge of the constitutive model they wish to fit to the existing measurement data. Industrial practice, however, shows that the available measurement data are often incomplete and contradictory, and the user does not have an advanced knowledge of the exact material behaviour.

The main goal of the pre-processing module (Fig. 2) is not only to select the suitable material models for fitting but also to provide information about the model parameters (min/max values and initial values) to speed up and improve the accuracy of the model fitting.

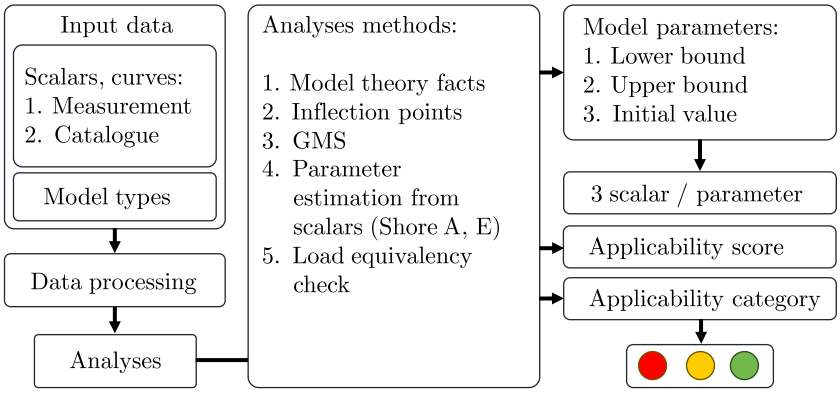

Fig. 2. Flowchart of the proposed data pre-processing module.

3.1. Analyses methods

The pre-processing module is based on the following five methods: 1) theoretical model properties; 2) inflection check; 3) GMS transformation; 4) parameter estimation from scalars, and 5) load equivalency check.

3.1.1. Theoretical model properties

In this module, the theoretical suitability of each material model is examined. Based on the previous list (see Subsection 2.3), it can be seen that the strain energy potential of some hyperelastic models is only a function of the invariant I_1, while other models also depend on the invariant I_2. As a general rule, it is assumed that

– for I_1-dependent material models, it is sufficient to fit for a single load case; the measured data from the other load cases will not provide additional information;

– for I_1- and I_2-dependent material models, it is necessary to fit at least two load cases. In this case, one of the measurements that is particularly recommended is the biaxial load curve since this will be the most dominant of the basic load cases for the I_2.

Furthermore, this module also includes the estimation of the parameter's initial values based on theoretical considerations, e.g., the requirement of positive initial moduli, consistency with Hooke's law and any further constraints related to the model definition. Based on this analysis, both initial values and boundaries are defined for the model parameters.

3.1.2. Inflection

In this module, the convexity and the number of inflection points of the theoretical models and the measurement datasets are analyzed and compared. Spline interpolation is applied to each measurement curve in the datasets to reduce the effect of noisy measurement data from which the convexity, inflection points, and their location can be determined analytically. After the analysis of the measurement curve, the hyperelastic models are then evaluated to decide whether or not they are capable of describing a measurement curve with such inflection properties. Based on the analysis of the theoretical model curves, it can be concluded that

- Neo–Hooke, Mooney–Rivlin models can be excluded if inflections are present in any curve;
- Arruda–Boyce, 1-order Ogden models can be excluded if inflections are found in the compression range, in simple shear, or if more than one inflection is seen in the tensile regime.

3.1.3. Generalized Mooney space transformation

The GMS transformation is a method developed recently by Anssari-Benam *et al.* (2022) as an extension of the Mooney–Rivlin plot. For the simpler hyperelastic models (Neo–Hookean, Mooney–Rivlin, Yeoh, Gent), the stress-strain curve ($P(\lambda) \to \mathcal{G}(\eta)$) can be transformed to a GMS of the material model, where the stress-strain curve for the simpler material models can be rewritten in a polynomial form. For the pre-processing module, this method is used in several ways.

Firstly, it allows for checking the suitability of the model to characterize the measurements. This can be easily checked using the polynomial space transformation, where the applicability of simpler models can be examined. If the GMS transform of the measurement curve matches the nature of the theoretical curve, the model can be adequate, i.e., it should be recommended for fitting. If the GMS transform of the measurement curve contradicts the nature of the theoretical curve, the given model will be excluded from the list of suitable strain energy functions.

Moreover, parameter fitting in a polynomial space is also much more reliable and robust. As a result, after transforming each material model into a GMS, a fast polynomial fitting can be used to estimate the initial value of the material parameters. The drawback of this method is that GMS transformation is not available for complex material models.

3.1.4. Parameter estimation from scalars

In addition to the measurement curves performed from material testing, the mechanical behaviour of the investigated elastomer can also be characterized by scalar parameters, which are often available as catalogue data, e.g., on the material data sheet. Such scalar values may be the modulus at 100 % elongation E_{100}, the modulus at 200 % elongation E_{200} or the modulus at 300% elongation E_{300}, which are commonly used in polymer technology. These quantities can be easily converted to material parameter relationships by evaluating the stress solutions at the given stretch level, respectively, to the given elongation level. In the proposed pre-processing module, we can use these scalar modulus values to estimate the initial values of the material parameters. Another important metric in the field of elastomers is the Shore A hardness, an easy-to-perform measurement that is often available in catalogue data. Using Qi's model (Qi *et al.*, 2003), which relates the Shore A hardness H_A and the elastic modulus as

$$\lg E = 0.0253 \cdot H_A - 0.6403 \qquad \text{for} \qquad 20 < H_A < 80, \tag{3.1}$$

we can estimate the initial elastic modulus of the material, from which we can also estimate the initial value of the model parameters using the above relationships.

3.1.5. Load equivalency check

It can be shown that due to the incompressibility, some load cases can be considered equivalent from a theoretical viewpoint since by adding or removing any hydrostatic pressure (see Eq. (2.6)), the deformation of the specimen does not change. Therefore, the load case pairs of uniaxial tension – biaxial compression and uniaxial compression – biaxial tension can be considered as equivalent load cases. Furthermore, this also means that if both tension and compression data are available for uniaxial or biaxial load cases, one already has two non-equivalent measurements. In this module, the load equivalency is analyzed. This module is used to analyze equivalent load cases, i.e., to check the consistency of the data from the cases considered equivalent. In the case of a discrepancy above a threshold value, the user is warned.

3.2. Evaluation of the pre-processing

By utilizing the methods mentioned above, the pre-processing module will provide: a) lower and upper bounds for the model parameters, b) initial values for some of the parameters, and c) an evaluation of model suitability using the traffic light marking system. Based on the pre-processing results, this classifies the available material models into the following categories:

- red – there is a discrepancy between the material model and the uploaded measurement data. This material model is not recommended for fitting;
- yellow – there is no inconsistency between the material model and the uploaded measurement data, but the uploaded data is incomplete for adequate fitting;
- green – no inconsistency between the given material model and the measurement data.

As a last step in the pre-processing module, a quick fitting is performed for each curve separately in order to quantify the accuracy of the model. Based on the preliminary single-curve fitting results and all the further pre-processing results, an applicability score is generated for each material model in the range of [0, 10], where 10 indicates the perfect match.

4. Case-studies

In order to highlight the benefits of the proposed pre-processing algorithm, two case studies were performed, including 1) the well-known Treloar dataset (Treloar, 1944) for unfilled rubber and 2) a self-made measurement dataset for a NBR specimen.

4.1. Measurement data I – Treloar-data

The first set of measurement data was the well-known Treloar dataset (Treloar, 1944) for unfilled rubber, which includes mechanical tests for three different load cases, namely uniaxial (UA), biaxial (BA) and planar (PL) tension. The $P - \lambda$ engineering stress (forces-per-initial cross-sectional area) – stretch dataset is depicted in Fig. 3.

4.2. Case study II – NBR

The second dataset (eCon measurement) contains measurements conducted at the test laboratory of eCon Engineering Ltd. The test specimens were made out of NBR. The four different load cases in the measurement set were: a) uniaxial tension (UT), b) uniaxial compression (UC), c) planar tension (PT), and d) simple shear (SS). The uniaxial tensile measurement was carried out according to the ASTM 412 standard (see Fig. 4) using an INSTRON 8801 servo-hydraulic Material Testing System equipped with a Dynacell 2527-111 100 kN load cell. The uniaxial compression test was performed according to ASTM D395. The specimen measured was made up of 3 rubber disks piled on each other, as shown in Fig. 4. For the planar tension test, there were no standards to follow, but a fairly common approach is to use a “wide enough”, thin, rectangular specimen with both of its ends fastened in a test frame as displayed in Fig. 4. A uniaxial test

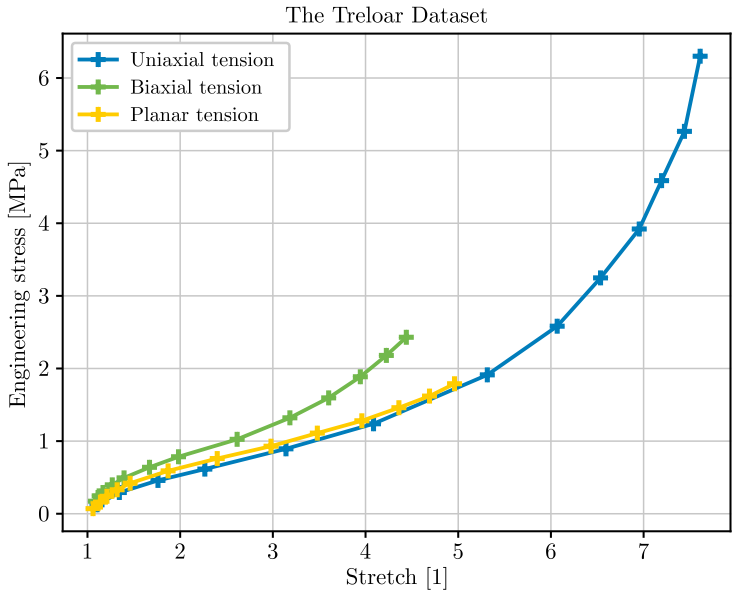

Fig. 3. $P - \lambda$ engineering stress (force-per-initial cross-sectional area) – stretch curves of uniaxial, biaxial and planar tension data from the Treloar dataset (Treloar, 1944).

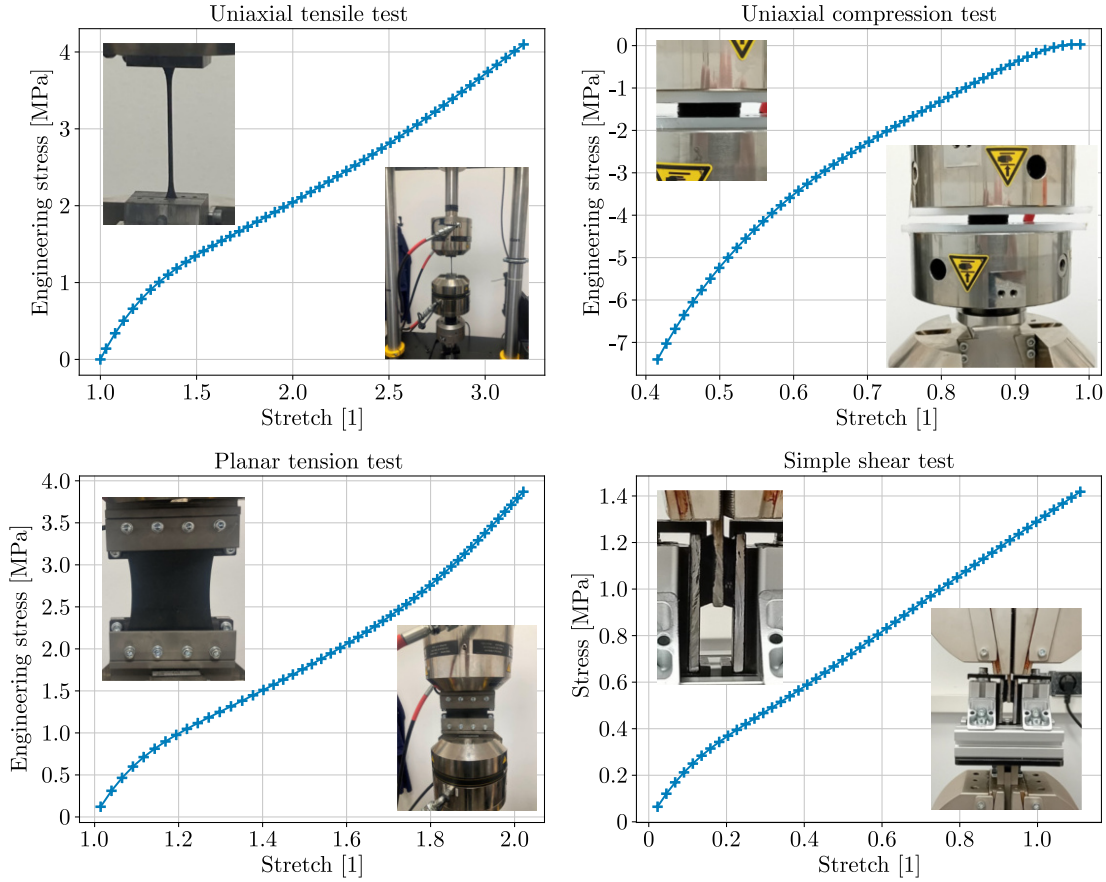

Fig. 4. Uniaxial tension, uniaxial compression, planar tension and simple shear measurement curves for the investigated NBR specimen.

machine can then pull the frame at both ends. Finally, a simple shear test according to ASTM D945 was also performed using a H&P universal testing machine with H&P 50 kN load cell, as shown in Fig. 4. The planar and simple shear measurements were performed using custom designed and manufactured grippers.

4.3. Parameter fitting scenarios

Both the pre-processing algorithms and the fitting tool were implemented in Python, the latter software component relying heavily on the "lmfit" Python package (Newville *et al.*, 2024). The possible benefits of using our pre-processor were examined by comparing the obtained fitted results, initializing all parameters with a) the constant value of 1 (Inits:1) or b) random numbers (Inits: rnd).

For the demonstration of the capabilities of the proposed algorithms, five different models from three different model families (see Fig. 1) were used with both datasets. These were the stretch ratio-based 2nd and 3rd-order Ogden models (O2 and O3), the Neo–Hookean (NH) and 3rd-order polynomial (PL3) and the Arruda–Boyce (AB) model from the statistical-mechanical model family. All five models were fitted on both datasets with constant 1 (Inits:1) and randomly generated numbers (Inits: rnd) as starting model parameter initial values and with and without using the pre-processing algorithms.

4.4. Fitting results

The remaining residuals after the fitting are displayed for all models at the top of Fig. 5 for the Treloar dataset and Fig. 6 for the eCon measurements. The colour of the circles above the residual bar charts indicates whether the pre-processor found the model applicable or not. The scores next to the circles show how good the fitting quality will be, based on the algorithm's estimation before the actual fit happens.

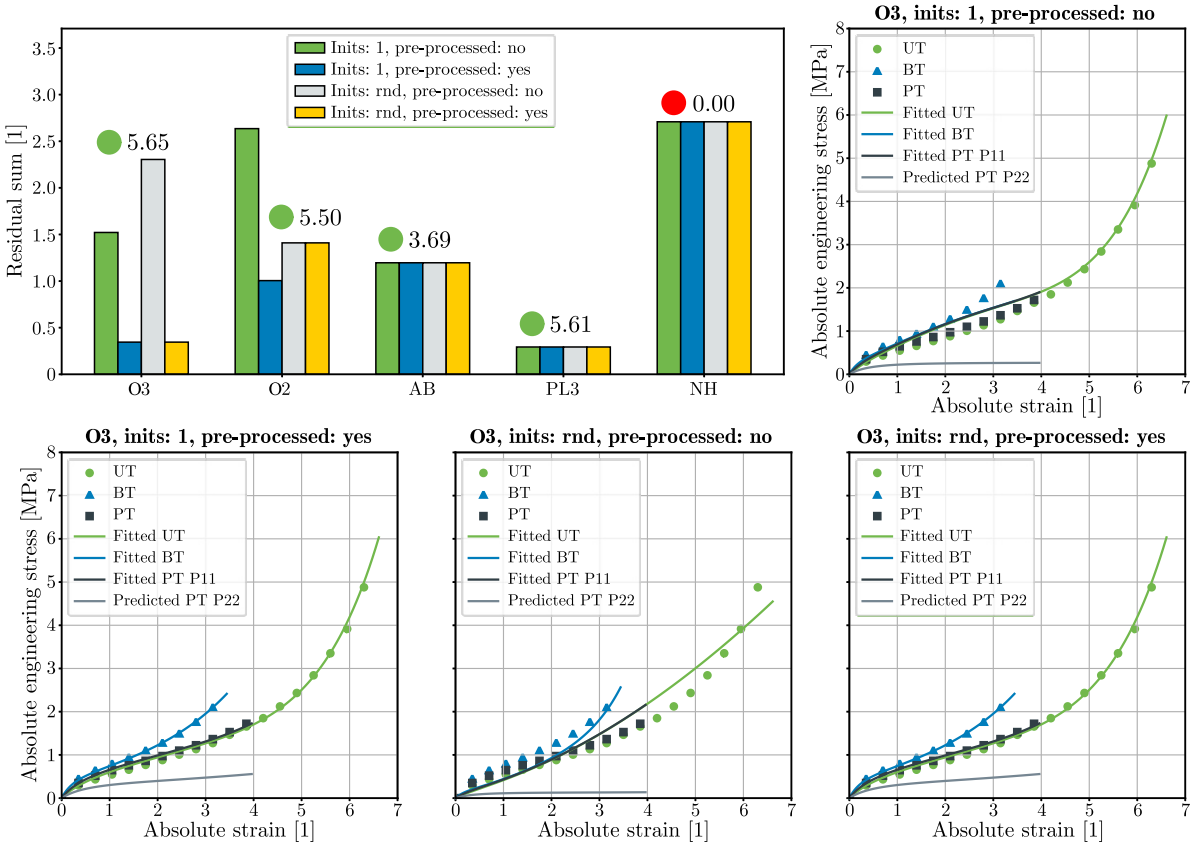

Fig. 5. Fitting results for the Treloar dataset using four fitting scenarios including the 2nd and 3rd-order Ogden models (O2 and O3), the Neo–Hookean (NH) and 3rd-order polynomial (PL3) and the Arruda–Boyce (AB) models.

As the summaries of the residual plots show, the applicability scores from the pre-processor show great agreement with the residual sums after the complete fitting procedure with one ex-

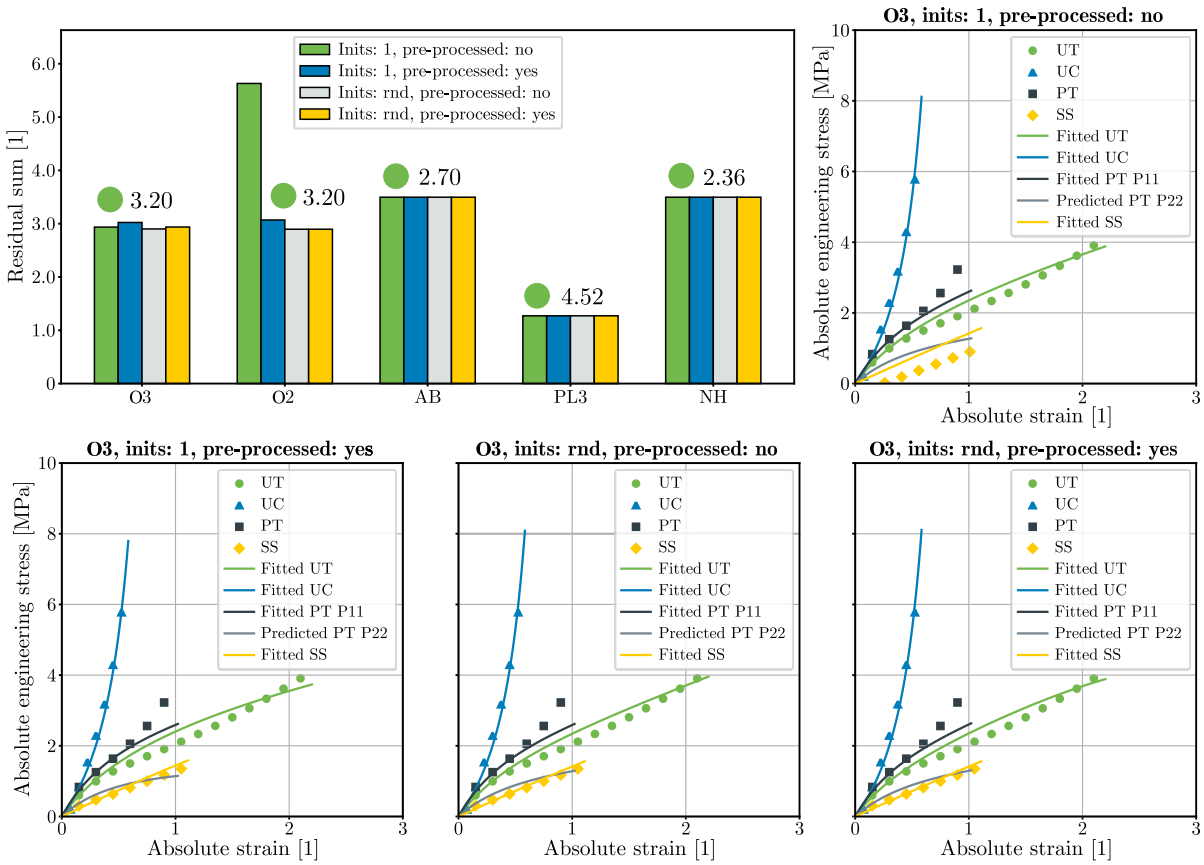

Fig. 6. Fitting results for the eCon dataset using four fitting scenarios including the 2nd and 3rd-order Ogden models (O2 and O3), the Neo–Hookean (NH) and 3rd-order polynomial (PL3) and the Arruda–Boyce (AB) models.

ception: in the case of the Treloar dataset, the 2nd order Ogden model ended up with a higher remaining residual value than the Arruda–Boyce model when the model parameters were randomly initialized. The Neo–Hookean model was also correctly identified as non-applicable (red circle) in the case of the Treloar dataset since it could not describe the inflections present in the measured curves.

Considering the effect of the initial values provided by the pre-processing algorithms, it was found that for models where the model redundancy was high (parameters can take each other's role), e.g., in the case of the 3rd order Ogden model, the suggested initial values for the parameters were able to improve the fitting accuracy. For this model, the obtained curves and the measurement data were plotted against each other on the bottom part of Fig. 5 and Fig. 6. for all four fitting scenarios. As one can see, the improvements in the fit quality in the Treloar dataset case were high. For the other models, the differences between the pre-processed and simple fits were not significant in any of the scenarios.

5. Conclusion

This paper presents a pre-processing procedure for incompressible hyperelastic fitting of rubber-like materials. The proposed method, based on the analysis of the measurement curves and the theoretical background of each hyperelastic model, not only provides an estimate of the initial values and bounds of the model parameters but also evaluates the adequacy of each material model. This provides the user with a tool to assist in choosing a material model. The performance of the method is illustrated via two case studies using the Treloar dataset and an NBR dataset.

As detailed in the previous section, the proposed pre-processing algorithms provided a very decent, although not completely errorless, assessment of the different models' applicability and expected fit quality upfront. Furthermore, the offered initial values significantly improved the final quality of the fit in some cases. However, they did not lead to significantly faster fitting times. For hyperelastic models with a high number of parameters, the minimization of the objective function can result in multiple solutions with similar goodness (local minima) due to the redundancy of the terms in such constitutive models. With a good choice of initial values, i.e., with physically consistent initial values, such redundancy of fitting results, and thus the uncertainty of the fitting can be reduced. Such initial values can usually be defined for the parameters related to the lower terms in the strain energy function. Therefore, in the case of models with a higher number of parameters (e.g., 3rd-order polynomial (PL3), 3rd-order Ogden models (O3)) specifying constraints and initial values to improve the uniqueness of the fit is still a challenge to be solved in future research.

It was also found that the pre-processing step greatly improved the fitting accuracy for models where the model redundancy was high (parameters can take each other's role), e.g., in the case of the 3rd-order Ogden model. For less complex models, the differences were not significant. The initial values provided by the pre-processor are close to the values obtained after the fitting process. However, this did not bring significant improvements in the fitting runtimes for the examined models. The randomly initialized cases were executed without noticeable differences. However, having good initial guesses can significantly improve runtimes in more complex models (e.g., compressible or viscoelastic models).

Acknowledgments

This research activity has been completed with the grant from the National Research, Development and Innovation Office. The project title is as follows: Precision Characterization of Nonlinear Mechanical Behaviour of Reinforced and Unreinforced Polymeric Materials for Numerical Simulations (project number: 2020-1.1.2-Piaci-KFI-2021-00314). Szabolcs Berezvai has been supported by the Hungarian National Research, Development and Innovation Office (NKFIH NKKP STARTING 149473) and the Janos Bolyai Research Scholarship of the Hungarian Academy of Sciences.

References

1. Anssari-Benam, A., Bucchi, A., Destrade, M., & Saccomandi, G. (2022). The generalised Mooney space for modelling the response of rubber-like materials. *Journal of Elasticity*, *151*(1), 127–141. https://doi.org/10.1007/s10659-022-09889-1
2. Arruda, E.M., & Boyce, M.C. (1993). A three-dimensional constitutive model for the large stretch behavior of rubber elastic materials. *Journal of the Mechanics and Physics of Solids*, *41*(2), 389–412, https://doi.org/10.1016/0022-5096(93)90013-6
3. Bergström, J. (2015). *Mechanics of solid polymers. Theory and computational modeling.* William Andrew.
4. Doghri, I. (2000). *Mechanics of deformable solids. Linear and nonlinear, analytical and computational aspects.* Springer Berlin Heidelberg. https://doi.org/10.1007/978-3-662-04168-0
5. Gent, A.N. (1996). A new constitutive relation for rubber. *Rubber Chemistry and Technology*, *69*(1), 59–61. https://doi.org/10.5254/1.3538357
6. Gent, A.N., & Thomas, A.G. (1958). Forms for the stored (strain) energy function for vulcanized rubber. *Journal of Polymer Science*, *28*(118), 625–628. https://doi.org/10.1002/pol.1958.1202811814
7. He, H., Zhang, Q., Zhang, Y., Chen, J., Zhang, L., & Li, F. (2022). A comparative study of 85 hyperelastic constitutive models for both unfilled rubber and highly filled rubber nanocomposite material. *Nano Materials Science*, *4*(2), 64–82. https://doi.org/10.1016/j.nanoms.2021.07.003

8. Holzapfel, G.A. (2010). *Nonlinear solid mechanics: a continuum approach for engineering*. Wiley.
9. Mooney, M. (1940). A theory of large elastic deformation. *Journal of Applied Physics*, *11*(9), 582–592. https://doi.org/10.1063/1.1712836
10. Newville, M., Otten, R., Nelson, A., Stensitzki, T., Ingargiola, A., Allan, D., Fox, A., Carter, F., Michał, Osborn, R., Pustakhod, D., Weigand, S., lneuhaus, Aristov, A., Glenn, Mark, mgunyho, Deil, C., Hansen, A.L.R., ... Persaud, A. (2024). lmfit/lmfit-py: 1.3.2 (1.3.2). Zenodo. https://doi.org/10.5281/zenodo.12785036
11. Ogden, R.W. (1972). Large deformation isotropic elasticity – on the correlation of theory and experiment for incompressible rubberlike solids. *Proceedings of the Royal Society A. Mathematical, Physical and Engineering Sciences*, *326*(1567), 565–584. https://doi.org/10.1098/rspa.1972.0026
12. Qi, H.J., Joyce, K., & Boyce, M.C. (2003). Durometer hardness and the stress-strain behavior of elastomeric materials. *Rubber Chemistry and Technology*, *76*(2), 419–435. https://doi.org/10.5254/1.3547752
13. Rivlin, R.S., & Saunders, D.W. (1951). Large elastic deformations of isotropic materials VII. Experiments on the deformation of rubber. *Philosophical Transactions of the Royal Society A. Mathematical, Physical and Engineering Sciences*, *243*(865), 251–288. https://doi.org/10.1098/rsta.1951.0004
14. Treloar, L.R.G. (1944). Stress-strain data for vulcanised rubber under various types of deformation. *Transactions of the Faraday Society*, *40*, 59–70. https://doi.org/10.1039/tf9444000059
15. Treloar, L.R.G. (2005). *The physics of rubber elasticity* (3rd ed.). Oxford Classic Texts in the Physical Sciences. Oxford University Press.
16. Yeoh, O.H. (1990). Characterization of elastic properties of carbon-black-filled rubber vulcanizates. *Rubber Chemistry and Technology*, *63*(5), 792–805. https://doi.org/10.5254/1.3538289

Manuscript received December 14, 2024; accepted for publication May 19, 2025; published online June 25, 2025.